AN ANALYTICAL SUPERSTEM FOR EXTRATERRESTRIAL MATERIALS RESEARCH. J. P. Bradley[1], Z. R. Dai[1], M. Wall[1], R. Erni[2] and N. Browning[2,3], [1]Institute for Geophysics and Planetary Physics, Lawrence Livermore National Laboratory, Livermore, CA 94551, USA (jbradley@igpp.ucllnl.org), [2]Department of Chemical Engineering and Materials Science, University of California Davis, Davis, CA 95616, USA, [3]National Center for Electron Microscopy (NCEM), Lawrence Berkeley National Laboratory, Berkeley, CA 94720, USA.

Introduction: A next generation analytical transmission electron microscope known generically as "SuperSTEM" is being funded jointly by NASA's SRLIDAP program and Lawrence Livermore National Laboratory (LLNL). Anticipated key features of the SuperSTEM are a monochromator, high-resolution electron energy-loss spectrometer, dual spherical aberration (Cs) correctors, novel solid-state x-ray detector technology, and specimen stage compatibility with the nanoSIMS. The monochromator reduces energy spread in the electron probe from ~1 eV to ~0.1 eV (Figs. 1-3), while Cs correctors improve image resolution and increase probe current (~10X) in atom-sized probes [1,2]. Analytical capabilities of the SuperSTEM will include atomic-resolution Z-contrast imaging, atomic-scale mineralogical and petrographic mapping, and electron spectroscopy with energy resolution comparable to synchrotron XANES (≤0.1 eV) but with >100X improved spatial resolution. An interim 200 keV instrument equipped with a monochromator will be installed at LLNL in May 2004, and a final 200 or 300 keV instrument with monochromator and Cs correctors will be installed in early 2006. The SuperSTEM, NanoSIMS, dual beam focused ion beam (FIB) instrument, ultramicrotome, and a cleanroom at LLNL will be available to the meteoritics community for analysis of meteoritic materials, cometary and interstellar dust particles from the Stardust mission, and returned samples from other current and planned missions (e.g. Hyabusa and Gulliver).

Technical: Our experience with IDPs suggests that a significant fraction of the STARDUST particles will be heterogeneous aggregates of carbonaceous matter, glass, and crystals with a grain size on the order of 2-5 nm. Understanding the basic petrography of such complex assemblages will require compositional mapping with spatial resolution of ~2nm or better. Such maps can be obtained from thin specimens using x-ray mapping, electron energy-loss mapping, or energy-filtered imaging. X-ray mapping is inherently simple and potentially quantitative but low x-ray count rates from thin specimens demand acquisition times on the order of an hour or more for ~100 nm^2 areas of thin specimens. LLNL is designing a high solid-angle detector that may enable increased x-ray count rates. Energy-filtered imaging is rapid (with acquisition times on the order of seconds) with high signal-to-noise, but quantification is less straightforward. Nonetheless, energy-filtered images can provide the ability to observe the petrography of chondritic IDPs with spatial resolution better than the average grain size (Fig. 4).

Results: We present here preliminary electron energy-loss data from a monochromated 200 keV STEM (Tecnai G^2) as well as high spatial resolution compositional mapping data using energy filtered imaging.

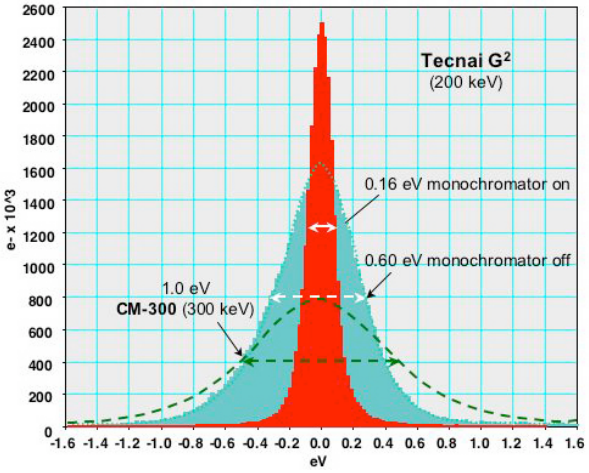

Figure 1 Comparison of energy resolution on zero-loss peak at 300 keV (green dashed line), at 200 keV with monochromator off (blue), at 200 keV with monochromator on (red).

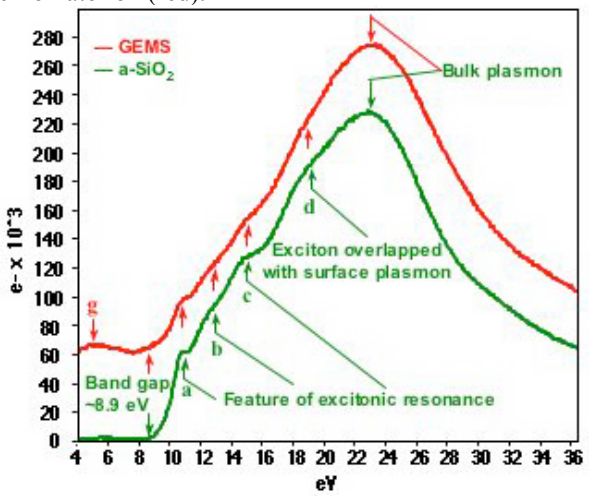

Figure 2 Electron energy-loss spectra of the low-loss region of amorphous silica-SiO_2 (green line) and GEMS (red line) showing similar interband transitions and excitonic resonances (a-d), monochromator on.

Figure 1 compares zero loss peaks acquired using Schottky field emission guns. At 300 keV energy resolution is ~1 eV (FWHM). At 200 keV energy resolution is improved by a factor of ~5 (from 0.6 to 0.16 eV) using the monochromator and a high-resolution electron energy-loss spectrometer. Our target energy resolution for routine analytical applications is ≤0.1 eV. The utility of improved energy resolution is illustrated in Figure 2 where the low-loss region of amorphous SiO_2 is compared with the glassy Mg-silicate matrices of GEMS. Although GEMS are stoichiometrically enriched in O [3], their electronic modes of excitation are similar to those of SiO_2 (Fig. 2). It has been proposed that the large bulk O excesses in GEMS (≤ 60 atomic %) are due to –OH [3]. New evidence in support of this hypothesis is shown in Figure 3. The inset is a bright field image of a vesicle-rich amorphous silica grain in IDP W7013E-17. All of the amorphous silicates, including GEMS, in this IDP are vesiculated, suggesting partial thermal decomposition during atmospheric entry. Electron energy-loss spectra of O-K edges from the vesicles were compared with O-K edges from the surrounding glass. Some vesicles produce a strong O-K pre-edge absorption feature (Fig 3a) while others do not (Fig. 3b). A similar less intense pre-edge feature can be detected in GEMS (Fig. 3c) [3]. This O-K pre-edge structure is consistent with molecular H_2O [4]. The specimen was cooled to –176 ^oC using a cold stage. Electron diffraction patterns obtained from the vesicles yielded reflection rings with spacings of 1.94 Å and 1.45 Å consistent with cubic ice. A third ring at 2.46 Å is unidentified.

It has been reported that non-solar O isotope abundances in GEMS and crystalline silicates establish the presence of presolar silicates in IDPs [5]. But GEMS contain two forms of O (Fig. 3a&b), and the crystalline silicates in IDPs are often admixed or coated with amorphous silicates with compositions similar to the Mg-rich glassy matrices of GEMS. It is possible that the reported O anomalies are carried by loosely bound secondary –OH and/or H_2O and not by the silicates themselves. This ambiguity underscores our effort to develop high-precision NanoSIMS/ superSTEM stage compatibility such that isotope measurements can be accurately correlated with the nanometer-scale mineralogy of chondritic IDPs.

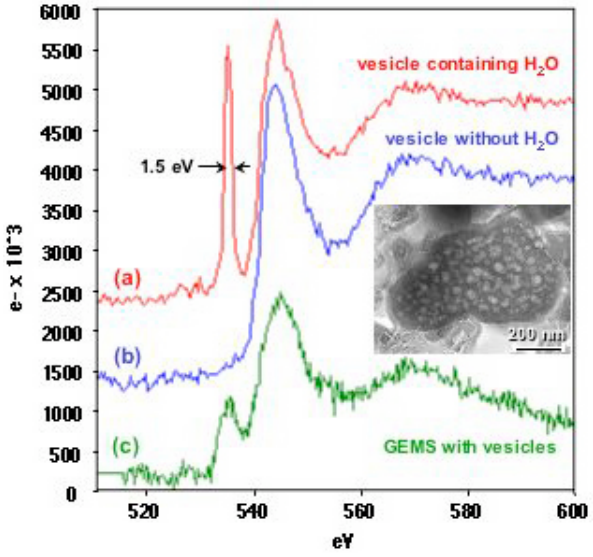

Figure 3 (Inset) 300 keV brightfield image of a silica grain with vesicles in IDP W7013E17. Spectra (top to bottom) are oxygen-K core ionization edges from (a) vesicle with H_2O, (b) without H_2O, and (c) GEMS.

Figure 4 illustrates the use of energy filtered imaging for investigating mineralogy and petrography at the nanometer-scale. Figure 4a shows a zero-loss image of a reduced aggregate (RA) [6] in IDP "Butterfly" that contains kamacite (FeNi metal) crystals with hematite (Fe_2O_3) rims embedded within carbonaceous matrix. There is a gap ~ 20 Å wide between the rims and the crystals (Figs. 4b & 4d). Figures 4c and 4d are mosaic energy-filtered maps formed from C-K (blue), O-K (red), and Fe-$L_{2,3}$ (green) element mappings. The gap between the metal grain and hematite coating is clearly resolved in Figure 4d, suggesting compositional spatial resolution of ~10 Å. The Fe_2O_3 rim presumably formed by oxidation of the metal grain, with the gap resulting from the lattice volume mismatch between the kamacite and hematite crystal structures.

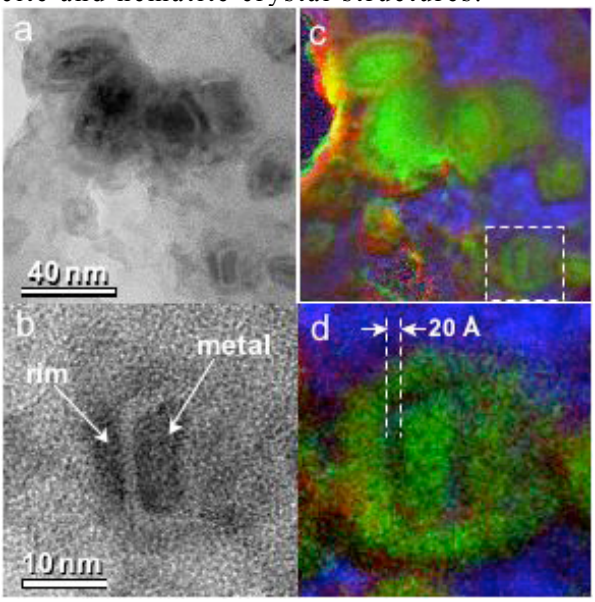

Figure 4 (a & b) Zero-loss energy filtered images of a reduced aggregate in IDP "Butterfly" (W7021 r21-m4-8a), (c & d) mosaic energy-filtered maps formed from C-K (blue), O-K (red), and Fe-$L_{2,3}$ (green) edges.

References: [1] Pennycook S. J., Rafferty B. and Nellist P. D. (2000) *Microsc. Microanal., 6,* 343–352. [2] Krivanek O. L. et al. (2003) *Ultramicroscopy* 96, 229-237. [3] Bradley J. P. (1994) *Science* 265, 925-929. [4] Parent Ph. et al. (2002) *JCP, 117,* 10842-10851. [5] Messenger, S. et al (2003) *Science* 300,105-108. [6] Bradley, J. P. (1994) *GCA*, 58, 2123-2134.